ACS Catalysis

pubs.acs.org/acscatalysis

Research Article

Plasma-Catalytic Ammonia Synthesis beyond the Equilibrium Limit

Prateek Mehta, Patrick M. Barboun, Yannick Engelmann, David B. Go, Annemie Bogaerts,* William F. Schneider,* and Jason C. Hicks*

Cite This: *ACS Catal.* 2020, 10, 6726−6734

Read Online

ACCESS | Metrics & More | Article Recommendations | Supporting Information

ABSTRACT: We explore the consequences of nonthermal plasma-activation on product yields in catalytic ammonia synthesis, a reaction that is equilibrium-limited at elevated temperatures. We employ a minimal microkinetic model that incorporates the influence of plasma-activation on N_2 dissociation rates to predict NH_3 yields into and across the equilibrium-limited regime. NH_3 yields are predicted to exceed bulk thermodynamic equilibrium limits on materials that are thermal-rate-limited by N_2 dissociation. In all cases, yields revert to bulk equilibrium at temperatures at which thermal reaction rates exceed plasma-activated ones. Beyond-equilibrium NH_3 yields are observed in a packed bed dielectric barrier discharge reactor and exhibit sensitivity to catalytic material choice in a way consistent with model predictions. The approach and results highlight the opportunity to exploit synergies between nonthermal plasmas and catalysts to affect transformations at conditions inaccessible through thermal routes.

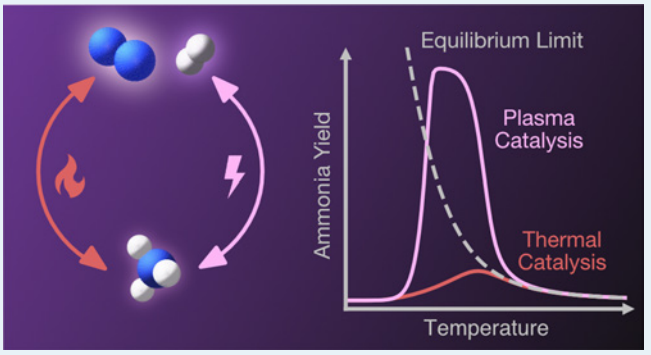

KEYWORDS: *plasma catalysis, nonthermal plasma, ammonia synthesis, thermodynamic equilibrium, kinetic modeling*

1. INTRODUCTION

A fundamental goal in catalysis is to obtain high yields of desired products at high production rates. In thermally driven catalytic systems, the reaction conditions under which this goal can be accomplished are constrained by the kinetic activity of the catalyst and the thermodynamics of the reaction. For many important reactions, these constraints can only be satisfied at severe conditions, particularly if they involve the transformation of unreactive molecules. As an example, consider the ammonia synthesis reaction from dinitrogen and hydrogen, $N_2 + 3H_2 \rightleftharpoons 2NH_3$. This reaction is exergonic at near-ambient conditions ($\Delta G°(298\ K) = -32.8\ kJ\ mol^{-1}$); thus, high yields are thermodynamically possible, but typical heterogeneous catalysts are inactive near ambient temperature.[1,2] Increasing the temperature into the regime in which catalytic turnover rates become appreciable also pushes the equilibrium of the exothermic reaction toward reactants, so that elevated pressures and recycle are necessary to achieve practically useful yields. Typical industrial-scale NH_3 synthesis processes thus operate at temperatures in the range 700−800 K and pressures in the range 100−200 atm.[1,3,4]

Recent reports have shown that ammonia synthesis can be performed at milder temperatures and pressures (~473 K, 1 atm) when catalysts are operated alongside nonthermal plasmas.[5−20] Such plasmas are characterized by a nonthermal distribution of energy between different degrees of freedom, such that high populations of reactive species (e.g., vibrationally or electronically excited molecules, as well as radicals and ions) are accessible without significantly increasing the bulk gas temperature.[21−24] In particular, nonthermally activated N_2 species can experience lower dissociation barriers on a catalyst surface.[25−30]

In previous work, we considered the consequences of nonthermal N_2 excitation on ammonia synthesis rates using a microkinetic model.[16] This model augmented well-established thermal catalytic ammonia synthesis steps with the dissociation of plasma-activated N_2 at the catalyst surface to predict volcano curves for NH_3 synthesis rates under plasma-stimulation. The model assumed the presence of a steady-state, nonthermal distribution of vibrationally excited molecules, parametrized on the N_2 vibrational temperature extracted from optical emission spectroscopic measurements of a dielectric barrier discharge (DBD) plasma.[16,17] Model predictions indicated that (1) nonthermal excitation of N_2 lifts the volcano, such that NH_3 synthesis rates per reaction site at mild conditions may approach those at thermal Haber−Bosch conditions, and (2) the optimal catalytic material shifts from Fe and Ru toward intrinsically less reactive materials, like Co or Ni. Additionally,

Received: February 9, 2020
Revised: May 14, 2020
Published: May 18, 2020

https://dx.doi.org/10.1021/acscatal.0c00684
ACS Catal. 2020, 10, 6726−6734

the model suggested that terrace sites on metal nanoparticles, which are inactive in thermal catalysis, may also become active in a plasma environment. These model predictions were qualitatively consistent with plasma-catalytic kinetic experiments performed in a differential flow DBD reactor, which showed elevated site-time yields of NH_3 at atmospheric pressure and 438 K, as well as a shift in optimal catalyst material.[16,18]

Site-normalized rates are intrinsically difficult to compare across catalysts because of their sensitivity to the identification and enumeration of reaction sites. Yields relative to bulk equilibrium, in contrast, are readily and unambiguously observable. A potential implication of nonthermal plasma-assisted reaction acceleration is access to product yields that exceed limits based on apparent bulk thermal equilibrium.[24,31,32] This "beyond-equilibrium" phenomenon has been observed in plasma-enhanced catalysis of the endothermic dry reforming of CH_4 with CO_2. In this case, product yields are observed to exceed equilibrium yields at low bulk gas temperatures in the presence of plasma with or without catalysts.[24,33−46] The contributions of the catalyst and plasma to observed product yields in the apparent equilibrium-limited regime are unclear. Product yields are typically observed to increase with increasing plasma power[34,37,39−44,47] but are insensitive to[33,37] or even decrease with increasing bulk gas temperatures.[38] Similarly, the introduction of catalyst packing into the reactor is reported sometimes to enhance[39,41,44,47−49] and sometimes to diminish overall yields[34,37,39,40,45,46,48,50] relative to plasma alone. Additionally, apparent beyond-equilibrium effects on product yields for endothermic reactions like dry reforming are difficult to disentangle from local heating (hot spots) of the catalyst surface or reactor walls by the plasma.[22,51]

To address this gap in understanding of the coupling of catalyst and plasma on observed yields in the apparent equilibrium-limited regime, here we propose an extension to the previously reported plasma catalysis microkinetic model[16] to predict trends in product yields and compare them to laboratory nonthermal plasma-catalytic experiments. In order to make the model tangible and to avoid the complications of interpreting experimental results for an endothermic reaction, we develop the model and perform experiments to test predictions in the context of exothermic NH_3 synthesis. We replace the steady-state approximation on plasma-generated nonthermal N_2 vibrational distributions with an explicit kinetic treatment of the rate of plasma-stimulated generation of excited species. We exercise the model across a range of conditions and assumed catalyst types to highlight conditions under which conversions can be expected to exceed apparent equilibrium and to explain the material choice on these excursions. We show that beyond-equilibrium behavior is expected to be most pronounced on materials for which N_2 dissociation is strongly rate-limiting (i.e., materials that bind N weakly) and at temperatures at which thermal rates do not outcompete the rates of the nonthermally excited processes. Plasma-catalytic experiments conducted in a DBD reactor display trends consistent with model predictions. NH_3 yields exceeding the bulk equilibrium limit are observed and are greater on materials with weaker N binding energies (e.g., Pt) that are inactive for thermal ammonia synthesis. Moreover, the experiments highlight the potential to tune performance by independent manipulation of the nonthermal and thermal rates—yields can be increased further past equilibrium by increasing the plasma power but re-equilibrate at high bulk temperatures where the thermal reaction pathways become dominant. The work highlights how nonthermal plasma catalysis offers different performance trade-offs compared to conventional thermal catalysis and offers further support for the contribution of plasma-induced promotion of N_2 dissociation to the observed plasma influence on catalytic NH_3 synthesis rates.

2. RESULTS AND DISCUSSION

2.1. Kinetic Model. Figure 1 shows a condensed scheme for the plasma-catalytic ammonia synthesis reaction. Blue arrows indicate the conventional thermal pathway for ammonia synthesis, which includes the dissociative chemisorption of N_2 onto the catalyst surface followed by its sequential reaction with adsorbed hydrogens to form NH_3.

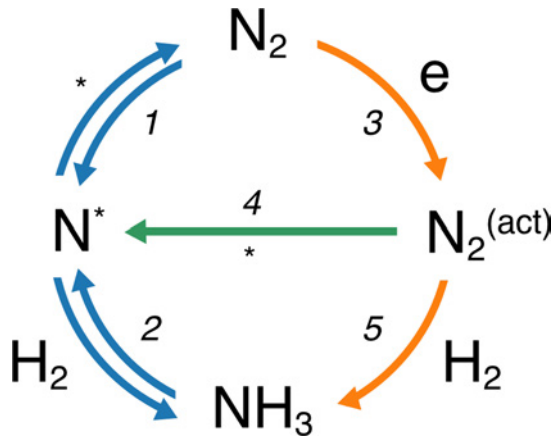

Figure 1. Reaction scheme for plasma-catalytic ammonia synthesis. The thermal reaction steps are shown with blue arrows. Homogeneous plasma-phase reactions are shown in orange. The plasma-catalytic adsorption of activated nitrogen is shown in green.

$$N_2 + 2^* \rightleftharpoons 2N^* \quad (1)$$

$$N^* + \frac{3}{2}H_2 \rightleftharpoons NH_3 + * \quad (2)$$

Here, * represents a catalytic site, and N* represents adsorbed nitrogen. The hydrogenation of N* typically occurs through a series of elementary steps involving the chemisorption of H_2 followed by the reaction of the adsorbed H* with NH_x* species (where x = 0, 1, 2). For convenience and with no loss of generality, these steps are lumped together in reaction 2.

Here, we assume that the primary plasma influence is to promote N_2 activation. Influences on H_2 activation are neglected, as such steps are accepted to be thermally rapid, consistent with the observed zero order rate dependence in H_2 in plasma-assisted NH_3 synthesis over Ni.[18] During plasma-driven operation, N_2 can be promoted by electron impact to a more reactive form, which we denote as $N_2^{(act)}$.

$$N_2 + e \rightarrow N_2^{(act)} + e \quad (3)$$

Reaction 3 is agnostic to the type of excitation—$N_2^{(act)}$ may be vibrationally or electronically excited, ionized, or even dissociated into N radicals depending on the energy of the colliding electron. In any of these forms, we consider activated

https://dx.doi.org/10.1021/acscatal.0c00684
ACS Catal. 2020, 10, 6726−6734

$N_2^{(act)}$ to chemisorb onto the catalytic surface (shown by the green arrow in Figure 1) with a smaller activation energy than that for reaction 1.

$$N_2^{(act)} + 2^* \rightarrow 2N^* \quad (4)$$

Assuming that N* primarily desorbs as ground-state N_2, reaction 4 becomes an irreversible step. In addition to the heterogeneous reaction pathway through reactions 4 and 2, the reactive $N_2^{(act)}$ species may participate in homogeneous plasma-phase reactions to form NH_3, as observed in plasma-only experiments (see refs 16, 18, and 24 and experiments discussed below). We write this reaction in a lumped fashion as

$$N_2^{(act)} + \frac{3}{2}H_2 \rightarrow NH_3 \quad (5)$$

The simple scheme depicted in Figure 1 allows us to develop a conceptual picture of plasma-catalytic NH_3 synthesis. Whether NH_3 is formed via thermal or nonthermal pathways depends on the relative rates along these pathways. When the rate of reaction 1, r_1, exceeds that of reaction 3, r_3, no benefits of plasma-stimulation of N_2 are expected; the reaction proceeds along the thermal pathway. Such a situation may arise at low specific electrical energy input, where the rate of plasma-driven activation of N_2 is low, or at high bulk temperatures, where thermal N_2 dissociation on the catalyst is rapid. Figure 1 neglects the quenching of plasma-activated species, which becomes increasingly important with increasing pressure and temperature. Similarly, nonthermal activation of N_2 does not impact catalytic reaction rates when the hydrogenation of surface adsorbed N* to NH_3 (reaction 2, r_2) is slow, as discussed in previous work.[16]

Plasma-driven reaction pathways become relevant when $r_1 \ll r_3$, and r_2 is not rate-limiting. If the generation of $N_2^{(act)}$ is slow relative to subsequent heterogeneous or homogeneous pathways, i.e., reaction 3 is rate-limiting, the reaction kinetics of plasma-only and plasma-catalytic operation become indistinguishable. If reaction 3 is not rate-limiting, the reaction is kinetically controlled by either reaction 4 or reaction 5. If r_5 is fast relative to $r_{4,2}$, NH_3 is formed predominantly via homogeneous plasma-phase mechanisms, and benefits of plasma-catalytic operation are not expected. This scenario may arise at low temperatures where surfaces are saturated by adsorbates, and higher gas pressures and/or low catalyst loadings, which favor reactive or dissipative homogeneous collisions of the excited states before they arrive at a catalytic site. Based on the above reasoning, the catalyst plays a kinetically significant role when the dissociation of $N_2^{(act)}$ on the catalytic surface is the rate-limiting step.

The electron impact activation of N_2 (reaction 3) is the primary driver of the nonthermal chemistry. We can write the net rate of $N_2^{(act)}$ generation as

$$r_3 = k_e n_e p_{N_2} \quad (6)$$

Here, n_e is the electron density, k_e is the electron impact rate coefficient, and p_{N_2} is the pressure of N_2. Both n_e and k_e depend on the characteristics of the nonthermal plasma.[21] k_e is primarily a function of the electron energy distribution function, or the effective electron temperature of the plasma, rather than the bulk temperature.

The rates of the forward and reverse processes in Figure 1 are thus controlled by different physical characteristics of the reacting system. The forward rate can be increased beyond what could be possible thermally by manipulation of the characteristics of the nonthermal stimulus; e.g., increasing the plasma power is expected to increase k_e and n_e and influence both the concentration of $N_2^{(act)}$ and its effective activation energy for further reaction. Additionally, because the forward and reverse processes are not connected by the principle of detailed balance, product yields will not be constrained by the equilibrium limitations characteristic of thermally driven reactions.[52]

To understand the implications of the decoupling of the forward and reverse rates on NH_3 yields, we implement the simple reaction scheme given by reactions 1–4 in a reactor model to trace reaction progress from the kinetic regime to the equilibrium-limited regime. Reaction 5 is not included in the model for simplicity and to isolate the catalytic consequences of nonthermal stimulation of N_2 on conversions. We model the system as a continuously stirred tank reactor (CSTR) operating at atmospheric pressure and constant volume (1 mL). The CSTR model is invariant in space (0D) and time and is convenient to represent the limiting behavior in the absence of transport or inhomogeneity effects. The reactants are introduced into the reactor in their stoichiometric ratio, at a flow rate of 10 mL min^{-1}. The overall volumetric flow rate decreases with reaction progression, because the reaction proceeds with a decrease in the number of moles. We consider that the reactor is packed with catalyst having only one type of active site (metal steps) with a total site density of 10^{-3} mol mL^{-1}.

We use the nitrogen binding energy (E_N) as a descriptor to calculate the rates of reactions 1 and 2. The activation energies for these reactions were calculated as a function of E_N using well-established Brønsted–Evans–Polanyi (BEP) relationships.[16,53,54] Because the hydrogenation steps are assumed to be unaffected by the plasma, they are treated in a lumped fashion[55] (as written in reaction 2). In this formulation, volcano curves for the reaction rates (see inset, Figure 2) still show the same general behavior as in previous work,[2,16,54,56]

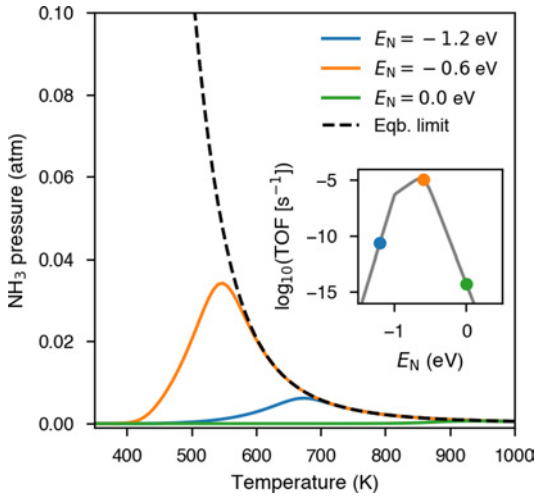

Figure 2. Modeled steady-state NH_3 partial pressures in thermal catalysis as a function of bulk temperature. Three catalysts are shown, characterized by strong (E_N = −1.2 eV), intermediate (E_N = −0.6 eV), and weak (E_N = 0.0 eV) nitrogen binding energies. The equilibrium pressure of NH_3 is shown by a dashed line. The inset shows the volcano curve for NH_3 synthesis calculated at 473 K, 1 atm, and 5% conversion of N_2.

https://dx.doi.org/10.1021/acscatal.0c00684
ACS Catal. 2020, 10, 6726–6734

although modeled rates are overestimated because N* is the only species included in the surface site balance. Further model details are available in Section 4.1 and the Supporting Information.

Figure 2 depicts the steady-state NH_3 pressure in the reactor as a function of the bulk temperature in the thermal catalysis model (i.e., excluding plasma reactions). Product yields are shown for three catalysts selected to span different characteristic regions (i.e., strong, intermediate, and weak N binding energies) of typical volcano curves. The catalyst that binds N with intermediate strength (E_N = −0.6 eV) sits at the top of the volcano curve (see inset) and provides the optimal balance between N_2 activation and its subsequent hydrogenation. This material thus displays the highest NH_3 yields of the three catalysts in Figure 2 at the specified reactor conditions. Ammonia yields increase with temperature until approaching the equilibrium limit, beyond which they follow the thermal equilibrium curve of diminishing NH_3 productivity with increasing temperature.

We next elaborate the CSTR model to incorporate activation of N_2 by a nonthermal plasma (i.e., reactions 3 and 4). To simplify the analysis, we include only one activated state in the model. Further, we assume that, upon excitation to this state, the N_2 dissociation barrier is reduced by 1 eV, corresponding to roughly three N_2 vibrational quanta. The extent to which the barrier is reduced is arbitrary and does not alter the qualitative conclusions of the work, as discussed in the Supporting Information (Figures S1 and S2).

We take the electron density (n_e) and the electron impact excitation rate constant (k_e, reaction 3) to be insensitive to the bulk temperature and gas composition. We scan over three representative values of the product $k_e n_e$, corresponding to a low, intermediate, and high rate of excitation. We neglect spatiotemporal variations in $k_e n_e$. However, we note that, in dielectric barrier discharge plasmas most commonly used for plasma catalysis, electron impact reactions are only expected to occur during short-lived (∼10 ns) filamentary microdischarges, followed by an afterglow period on the order of 1 μs.[57] To roughly account for the short-lived nature of the microdischarges and the much longer afterglow period, the $k_e n_e$ values used here are chosen to be smaller than or at the lower limit of the product of the k_e and n_e typical of DBD microdischarges (see the Computational Details section). To highlight the maximum possible plasma promotion effect on NH_3 yields, we neglect any potential plasma-promoted NH_3 decomposition pathways to N_2 and H_2. Plasma phase NH_3 decomposition has been reported,[58] and may limit maximum yields. Plasma-activation of NH_3 is not expected to promote decomposition rates on catalyst surfaces, because reactions between adsorbed species are typically rate-limiting in catalytic NH_3 decomposition.[59]

Figure 3 reports the steady-state NH_3 partial pressures as a function of the bulk temperature as predicted by the plasma-on CSTR model for the same three catalysts as above. The representative strong N-binding catalyst along the left leg of the thermal volcano curve (E_N = −1.2 eV) is presented in Figure 3a. Because this catalyst readily activates N_2, the reaction occurs via the thermal pathway, and no enhancements in NH_3 production during plasma-driven operation are observed. That is, the plasma-on product pressures correspond with the thermal-only results. During plasma-catalytic operation, the surface remains covered with N up to temperatures as high as 600 K, and substantial amounts of unreacted $N_2^{(act)}$ remain in the gas phase. These excited molecules could react along homogeneous pathways or relax and equilibrate with the bulk gas. Coupling of plasma and catalyst has no direct benefit in this case.

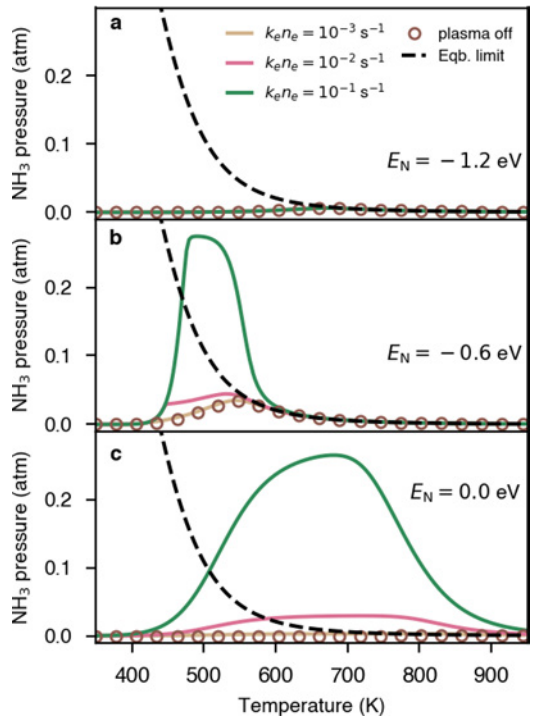

Figure 3. Modeled steady-state NH_3 partial pressures in plasma-enhanced catalytic operation as a function of bulk temperature and rate of plasma-excitation. Catalysts characterized by (a) strong (E_N = −1.2 eV), (b) intermediate (E_N = −0.6 eV), and (c) weak (E_N = 0.0 eV) nitrogen binding energies. For each catalyst, steady-state thermal (plasma-off) and plasma-on (for three values of $k_e n_e$) partial pressures of NH_3 are plotted. Plasma-excitation is assumed to reduce the barrier for N_2 dissociation by 1 eV.

Figure 3b,c plots NH_3 partial pressures for a material with near-optimal N binding energy for the thermal reaction (E_N = −0.6 eV) and for a material selected from the right leg of the thermal volcano curve (E_A = 0.0 eV), respectively. In the kinetic regime, the plasma-on models predict enhancements in NH_3 produced over thermal catalysis for both materials if the rate of plasma-activation of N_2 is sufficiently high ($k_e n_e \geq 10^{-2}$ s^{-1}). Results also indicate that plasma-on product pressures can exceed the bulk thermal-equilibrium limit on both of these materials. Further, the models indicate that the excursion from the thermal equilibrium curve is catalyst-dependent. For the optimal thermal catalyst, NH_3 yields exceeding equilibrium for the optimal thermal catalyst are observed at $k_e n_e = 10^{-1}$ s^{-1}, in the temperature window 475−600 K. In this temperature window, the amount of NH_3 produced first increases, reaches a maximum, and then collapses back to the equilibrium line. While the NH_3 yields show similar features as a function of the bulk temperature for the material that binds N more weakly than the optimal thermal catalyst, the degree of excitation required to observe beyond-equilibrium behavior is lower—NH_3 pressures are predicted to go beyond the equilibrium limit for $k_e n_e \geq 10^{-2}$ s^{-1}. Furthermore, the temperature range over which NH_3 pressures exceed the bulk equilibrium limit is significantly wider for this material.

https://dx.doi.org/10.1021/acscatal.0c00684
ACS Catal. 2020, 10, 6726−6734

We interpret the temperature-dependence of the NH_3 partial pressures for the two materials above as follows. Plasma-activation of N_2 facilitates its dissociative chemisorption on both materials at low temperatures, but slow hydrogenation at these temperatures limits its conversion to NH_3. Surface sites become available at temperatures ~400 K, resulting in light-off in the NH_3 pressures. Because the nonthermal pathway for N_2 dissociation (reactions 3 and 4) is decoupled from the thermal desorption of N* as N_2 (see Figure 1), product pressures can extend beyond the equilibrium limit. As the bulk temperature increases further, the steady-state partial pressures of NH_3 reach maxima and then decrease as the thermal rates along the reverse pathways become significant. Effectively, NH_3 formed via nonthermal pathways can be kinetically trapped at concentrations in excess of the bulk thermal equilibrium at lower temperatures, and catalysts drive these excess NH_3 yields back toward the bulk thermal equilibrium curve at higher temperatures. Because different catalysts become active for thermal ammonia decomposition at different temperatures, the steady-state NH_3 yields are catalyst dependent. At the temperature where NH_3 pressures converge on the bulk thermal equilibrium curve, the reaction occurs only through the thermal route; i.e., the rate of thermal N_2 dissociation exceeds the one along the plasma-induced pathway, and the net NH_3 yield is limited by the forward and backward rates of thermal NH_3 synthesis and decomposition. The reversion to the equilibrium curve occurs at lower temperature on materials closer to the thermal-only volcano maximum—the thermal rates in both the forward and backward directions are highest for this material.[60]

2.2. Experimental Section. We performed temperature-sweep experiments in a DBD reactor to investigate ammonia synthesis behavior near the equilibrium regime. The reactor was configured in a fashion similar to previous work[16−18,24] (further discussed in the Experimental Details section). We introduced the reactants into the reactor at a total flow rate of 40 sccm and a N_2:H_2 ratio of 2:1, which resulted in the highest NH_3 yields as determined in our previous work.[16,18] Initial experiments were performed to evaluate background contributions, plotted in Figure 4. These background measurements were made in a reactor packed with bare support material (100 mg γ-Al_2O_3), as opposed to an empty reactor, due to the potential of the dielectric packing to influence the discharge characteristics (plasma volume, discharge gap, etc.)[17,24] We note, however, that the empty reactor behaves similarly to the γ-Al_2O_3-packed reactor, as shown in Figure S4. The bulk reactor temperature was varied between 423 and 1123 K. Reaction performance was evaluated at plasma powers of 5, 10, and 15 W (the maximum allowable by our power supply), corresponding to specific energy inputs of 7.5, 15, and 22.5 kJ L^{-1}. In all experiments, we observed significant background NH_3 production, consistent with previous literature reports.[24] Furthermore, NH_3 production increased with increasing reactor temperature, and yields well beyond the equilibrium limit were observed at high bulk temperatures. In both the low- and high-temperature regimes, NH_3 yields increased with increasing plasma power. These experiments demonstrate that the plasma power can be used to manipulate the rates of the nonthermal reactions and drive the reaction further beyond the bulk thermal-equilibrium limit. At all plasma powers, NH_3 yields maximized at about 920 K, after which they decreased.

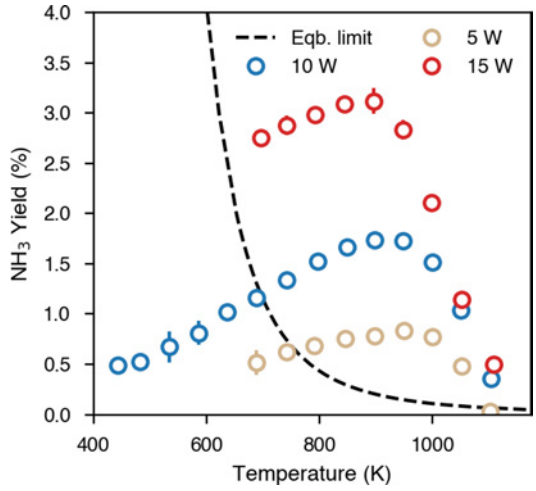

Figure 4. Plasma background ammonia yields in a DBD reactor packed with γ-Al_2O_3 as a function of bulk reactor temperature. Three powers, including 5, 10, and 15 W, are shown. Reaction conditions: total flow rate = 40 sccm, inlet N_2:H_2 = 2:1. The dashed line shows the bulk thermodynamic equilibrium conversion at the specified reaction conditions.

Next, we performed similar temperature-sweep experiments with the reactor loaded with Ni and Pt catalysts supported on γ-Al_2O_3 (100 mg of material, 5 wt % metal). We selected these materials because both bind N more weakly than the optimal thermal catalyst, Ru[2,16,54,56,61] (the N-metal bond strength follows the order Ru > Ni > Pt). Based on the kinetic analysis above, beyond-equilibrium behavior may be observable on these materials. In Figure 5a, we plot plasma-catalytic NH_3 yields on these two catalysts as a function of bulk gas temperature at 10 W plasma power. The corresponding NH_3 yields observed in the plasma reactor packed with only Al_2O_3 are included for comparison. In the low-temperature kinetic regime, the metal-based catalysts behave in a similar fashion—NH_3 yields increased with temperature on both materials, and both materials exhibited enhanced NH_3 production relative to the background. However, in the equilibrium-limited regime, the behavior of the two catalysts diverged significantly. On the Ni catalyst, NH_3 yields fell below those of the background experiment and collapsed onto the equilibrium curve. In contrast, temperature-sweep profiles on the Pt catalyst resembled those of the background experiment—NH_3 yields continued to increase with temperature, significantly exceeding the bulk equilibrium limit, before ultimately decreasing. Pt continued to enhance NH_3 production over the background at higher temperatures until about 1000 K, after which the yields converged.

The hypothesized reaction scheme in Figure 1 and the subsequent kinetic analysis suggest that the collapse of the NH_3 yields in Figure 5a is linked to the reaction proceeding in the reverse direction. To test the hypothesis, we performed thermal NH_3 decomposition experiments at feed compositions comparable to the outlet stream of the background experiment at 900 K (the temperature at which NH_3 yields were the highest). A gas mixture of 0.5% NH_3 and 9.5% He with a balance of N_2 and H_2 in a 2:1 ratio was fed into the reactor. Figure 5b plots the amount of NH_3 converted over the same three materials as a function of temperature. Of the tested materials, Ni/Al_2O_3 is the most active for NH_3 decomposition, lighting off at around 750 K. The decomposition curves for Pt/

https://dx.doi.org/10.1021/acscatal.0c00684
ACS Catal. 2020, 10, 6726−6734

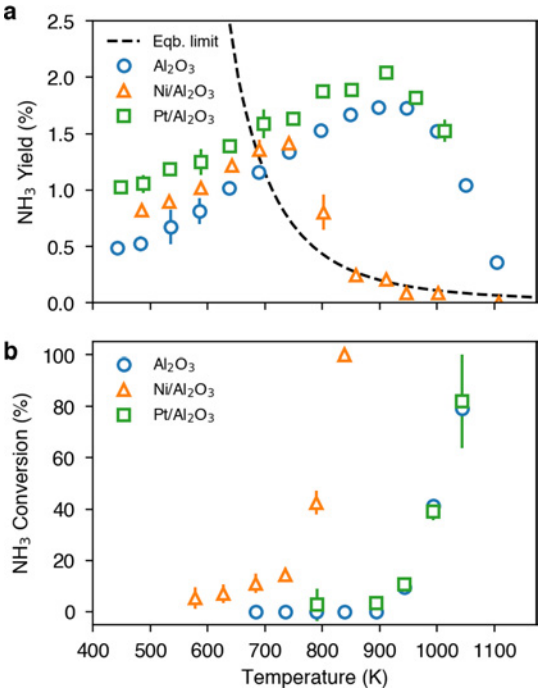

Figure 5. Ammonia synthesis and decomposition temperature-sweep experiments. (a) Plasma-catalytic ammonia yields in a DBD reactor packed with Al_2O_3, Ni/γ-Al_2O_3, and Pt/γ-Al_2O_3. Reaction conditions: total inlet flow rate = 40 mL min^{-1}, N_2:H_2 = 2:1. (b) NH_3 conversion in thermal ammonia decomposition experiments over γ-Al_2O_3, Ni/γ-Al_2O_3, and Pt/γ-Al_2O_3. Reaction conditions: Inlet flow rate = 40 mL min^{-1}. Inlet gas composition: 0.5% NH_3, 9.5% He, and balance of 2:1 N_2 and H_2.

γ-Al_2O_3 and metal-free γ-Al_2O_3 are nearly identical, lighting off at approximately 900 K. NH_3 is not stable at these high temperatures,[62] and we attribute the similarity of the light-off points for these two materials to gas-phase NH_3 decomposition (verified by comparison with empty reactor in Figure S5). The correspondence between the temperatures that NH_3 decomposition light off in Figure 5b and the collapse in the NH_3 synthesis yields in Figure 5a provides strong evidence of the decoupling of the thermally and nonthermally driven processes. Plasma-stimulated reactions allow access to yields of NH_3 in excess of bulk thermal-equilibrium limits. These excess ammonia yields can remain kinetically trapped until the temperature at which thermal NH_3 decomposition becomes kinetically relevant. The experiments thus support the model inference that the benefits of plasma-assisted NH_3 synthesis accrue most greatly for materials on the right (weaker binding) side of the thermal volcano plot, that they promote N* hydrogenation steps, and that performance with increasing temperature is limited by the reverse thermal NH_3 decomposition reaction.

3. CONCLUSIONS

The promise of plasma catalysis lies in the potential to carry out chemical conversions at conditions and with efficiencies that are inaccessible by thermal-only catalytic routes. Plasma-stimulation can in principle bypass kinetic bottlenecks in thermal-only catalytic transformations, enhancing net reaction rates and conversions. Here, we explore the consequences of plasma-stimulation across conditions at which thermal reactions become equilibrium-limited, in the context of ammonia synthesis, which under typical conditions is kinetically limited by the activation of N_2. We show that the presence of a nonthermally activated reaction channel can disturb the coupling of the forward and reverse rates; i.e., the forward and reverse rate processes balance each other at conditions different from those specified by the bulk thermal equilibrium. As a consequence, reaction products can be kinetically trapped in concentrations exceeding the equilibrium limit, as observed here for plasma-stimulated NH_3 synthesis. The contributions of the thermal and nonthermal channels may be independently manipulated by separate control of the bulk temperature and the plasma power (or the specific energy input), respectively. We find that, with increasing plasma power, ammonia yields extend further beyond the equilibrium limit, while yields re-equilibrate at temperatures at which thermal chemistry becomes dominant.

The model and experimental results further indicate that the extent of excursion from thermal equilibrium can be kinetically controlled by appropriate choice of catalytic material. The greatest departures are expected and observed on catalytic materials for which N_2 activation is strongly rate-limiting and thus are not optimal under equivalent thermal conditions. The above findings align with and support prior results that show that the greatest potential for kinetic enhancements is on catalysts that bind nitrogen weakly. Because NH_3 yields are measured with less ambiguity than turnover frequencies, the directional agreement between the kinetic model and the experiments provides strong evidence of a reaction mechanism that includes contributions from nonthermally activated N_2 dissociation. The overall energy efficiency of this process is thus a function of the efficiency at which plasma power is directed into reactant activation.

We chose here NH_3 synthesis as a model reaction because it is exothermic; any adventitious heating provided by the plasma will diminish rather than enhance NH_3 conversions, and conclusions regarding the influence of plasma-stimulation are thus not confounded by questions of temperature control. Similar concepts are expected to apply to endothermic reactions that are equilibrium-limited at low temperatures, such as methane dry reforming. Here, parallel plasma-promoted reaction channels will cause conversions to exceed bulk equilibrium at low temperatures and approach the thermal-equilibrium limit behavior at higher temperatures, as in fact is observed in experiments.[38]

4. METHODS

4.1. Computational Details. The ammonia synthesis reaction was modeled with $\Delta H(298\ K) = -91.8$ kJ mol^{-1}. Standard entropies of the gas phase N_2, H_2, and NH_3 were obtained from the National Institute of Standards and Technology (NIST) Chemistry WebBook (http://webbook.nist.gov/chemistry). The microkinetic model for the thermal reactions was developed using the approach of Grabow.[55] The rate expressions used for the reaction steps and Brønsted–Evans–Polanyi (BEP) relationships used to calculate activation energies are provided in the Supporting Information. To obtain an estimate of typical values of the electron density and the electron impact excitation rate coefficients, we solved the Boltzmann equation for a N_2 plasma at a reduced electric field of 100 Td[63] using the online solver at https://us.lxcat.net/. k_e typically ranges between 10^{-14} and 10^{-9} cm^3 s^{-1} depending on the type of excitation (e.g., vibrational or electronic excitation, ionization, etc.), while n_e is typically in the range 10^{14}–10^{15}

https://dx.doi.org/10.1021/acscatal.0c00684
ACS Catal. 2020, 10, 6726–6734

cm^{-3}. As noted in the main text, the electron impact reactions are only expected to occur during the short-lived DBD microdischarges, which exhibit spatial and temporal variations across the reactor. We ignore the temporal and spatial variations of the DBD plasma and assume that the product $k_e n_e$ can be treated as a constant independent of the bulk gas temperature. We scan the CSTR model over a number of representative values of $k_e n_e$, which are taken to be smaller than or at the lower limit of the product of the k_e and n_e values noted above, such that the model can crudely account for the long afterglow periods where the electron density is zero.

4.2. Experimental Details. Pt and Ni supported on γ-Al_2O_3 (5 wt %) were obtained from Riogen Inc. The structural properties of the catalysts were characterized prior to experiments. Surface areas were evaluated with N_2 physisorption using a Quantachrome 2200e instrument at 77 K. The crystallinity of the materials was evaluated using X-ray diffraction (XRD) over 30−70° 2θ using a D8 Advance diffractometer and referencing to a standard silicon crystal peak. Metal particle sizes were determined by transmission electron microscopy imaging using a Jeol 2011 electron microscope (images are provided in Figure S3). The average sizes of the Ni and Pt particles were approximately 15 and 2 nm, respectively. All particle sizes were based on at least 300 particles. In addition to physical properties, the number of accessible surface metal sites was evaluated both before and after the plasma reaction via CO pulse chemisorption using a Micromeritics Chemisorb 2750 instrument. Catalysts were pretreated in 20 sccm (standard cubic centimeter per minute) H_2 at 773 K for 30 min followed by 30 min in 20 sccm He at 773 K to remove chemisorbed H_2 and prevent potential polycarbonyl formation during CO adsorption. Characterization information can be found in Table S1.

The plasma reactor is the same as reported previously.[18,38,64] The reactor consists of a quartz tube (5 mm internal diameter and 1 mm wall thickness) wrapped in a stainless steel mesh (McMaster-Carr 200-1400) that covers 6 cm of the length of the tube and a 1.5 mm tungsten rod inserted through the center of the tube. Within this setup, the discharge gap is 1.75 mm, and the discharge volume is 1.07 cm^3. The plasma was generated by applying a high voltage from an AC power source (PVM500). Plasma power was maintained from 5−15 W using a driving frequency in the range 21−27 kHz. These conditions were monitored with an oscilloscope (Tetronix TDS3012B) using the Lissajous curve method described previously.[18,40] No significant changes in the $Q-V$ curves were observed across the temperature range studied, indicating that temperature did not significantly impact the plasma properties. Gas flow rates into the reactor were controlled using Aalborg GFC 17 mass flow controllers such that the flow rate of each gas could be controlled independently. For reactants, we used 99.999% N_2 (Airgas NI UHP300), 99.999% H_2 (Airgas HY UHP300), and 10% NH_3 in He (Airgas) with 99.997% He (Airgas HE HP300) occasionally used as a carrier gas or to purge the system. Gas chromatography (GC) measurements were calibrated using the 10% NH_3 in He gas mixture. The reaction temperature was externally controlled by a furnace over the temperature range 423−1123 K. Temperature was measured using a thermocouple downstream from the discharge zone that was calibrated *ex situ*. For each experiment, 100 mg of material was packed into the reactor. Each catalyst was pretreated at 773 K for 30 min in 20 sccm of H_2 before data collection. For each experiment the gas residence time of the reactants through the discharge zone was about 1.2 s using a flow rate of 40 sccm. We waited 15 min upon reaching each temperature point measured before doing GC injections in order to ensure that the reactor was at steady state prior to measurement. Each data point is based off of an average of three injections by the GC, and the error bars shown correspond to the standard deviation of these three measurements. Because the experiments were all conducted at low conversions (<4% even at the highest temperature evaluated), the composition of the gas stream was considered constant throughout the catalyst bed (i.e., differential conditions were assumed).

4.3. Data Availability. An external Zenodo repository hosts code and raw data.[65] The kinetic model and associated utility functions are included as Python files. Model input and calculated results are included in *json* format. Raw data for the plasma catalysis experiments is included in an Excel spreadsheet. Additional details and python scripts showing how these data files were used to create all the figures in the paper are provided in the Supporting Information.

■ ASSOCIATED CONTENT

Supporting Information

The Supporting Information is available free of charge at https://pubs.acs.org/doi/10.1021/acscatal.0c00684.

Additional computational details, catalyst characterization information, comparisons between empty and packed plasma reactors, Python examples of running the kinetic model, and code to reproduce all figures in the manuscript (PDF)

■ AUTHOR INFORMATION

Corresponding Authors

Annemie Bogaerts − *Department of Chemistry, Antwerp University, Antwerp 2610, Belgium;* orcid.org/0000-0001-9875-6460; Email: annemie.bogaerts@uantwerpen.be

William F. Schneider − *Department of Chemical and Biomolecular Engineering, University of Notre Dame, Notre Dame, Indiana 46556, United States;* orcid.org/0000-0003-0664-2138; Email: wschneider@nd.edu

Jason C. Hicks − *Department of Chemical and Biomolecular Engineering, University of Notre Dame, Notre Dame, Indiana 46556, United States;* orcid.org/0000-0002-5054-2874; Email: jhicks3@nd.edu

Authors

Prateek Mehta − *Department of Chemical and Biomolecular Engineering, University of Notre Dame, Notre Dame, Indiana 46556, United States;* orcid.org/0000-0001-6233-8072

Patrick M. Barboun − *Department of Chemical and Biomolecular Engineering, University of Notre Dame, Notre Dame, Indiana 46556, United States;* orcid.org/0000-0003-4214-462X

Yannick Engelmann − *Department of Chemistry, Antwerp University, Antwerp 2610, Belgium*

David B. Go − *Department of Chemical and Biomolecular Engineering and Department of Aerospace and Mechanical Engineering, University of Notre Dame, Notre Dame, Indiana 46556, United States;* orcid.org/0000-0001-8948-1442

Complete contact information is available at: https://pubs.acs.org/10.1021/acscatal.0c00684

https://dx.doi.org/10.1021/acscatal.0c00684
ACS Catal. 2020, 10, 6726−6734

Author Contributions

P.M. and P.M.B. contributed equally to this work. P.M. developed the kinetic model. P.M.B. performed ammonia synthesis experiments. All authors discussed the results and cowrote the manuscript.

Notes

The authors declare no competing financial interest.

■ ACKNOWLEDGMENTS

This work was supported by the U.S. Department of Energy, Office of Science, Basic Energy Sciences, Sustainable Ammonia Synthesis Program, under Award DE-SC-0016543 and by the U.S. Air Force Office of Scientific Research, under Award FA9550-18-1-0157. P.M. acknowledges support through the Eilers Graduate Fellowship for Energy Related Research from the University of Notre Dame. Computational resources were provided by the Notre Dame Center for Research Computing. We thank the Notre Dame Energy Materials Characterization Facility and the Notre Dame Integrated Imaging Facility for the use of the X-ray diffractometer and the transmission electron microscope, respectively.

■ REFERENCES

(1) Schlögl, R. *Handbook of Heterogeneous Catalysis*, 2nd ed.; Wiley-VCH Verlag GmbH & Co. KGaA, 2008; pp 2501−2575.
(2) Vojvodic, A.; Medford, A. J.; Studt, F.; Abild-Pedersen, F.; Khan, T. S.; Bligaard, T.; Nørskov, J. Exploring the Limits: A Low-Pressure, Low-Temperature Haber-Bosch Process. *Chem. Phys. Lett.* **2014**, *598*, 108−112.
(3) Ertl, G. *Catalytic ammonia synthesis*; Springer, 1991; pp 109−132.
(4) Nørskov, J.; Chen, J.; Miranda, R.; Fitzsimmons, T.; Stack, R. *Sustainable Ammonia Synthesis−Exploring the scientific challenges associated with discovering alternative, sustainable processes for ammonia production*; US DOE Office of Science, 2016.
(5) Mizushima, T.; Matsumoto, K.; ichi Sugoh, J.; Ohkita, H.; Kakuta, N. Tubular Membrane-Like Catalyst for Reactor With Dielectric-Barrier-Discharge Plasma and Its Performance in Ammonia Synthesis. *Appl. Catal., A* **2004**, *265*, 53−59.
(6) Mizushima, T.; Matsumoto, K.; Ohkita, H.; Kakuta, N. Catalytic Effects of Metal-Loaded Membrane-Like Alumina Tubes on Ammonia Synthesis in Atmospheric Pressure Plasma By Dielectric Barrier Discharge. *Plasma Chem. Plasma Process.* **2007**, *27*, 1−11.
(7) Kim, H.-H.; Teramoto, Y.; Ogata, A.; Takagi, H.; Nanba, T. Atmospheric-Pressure Nonthermal Plasma Synthesis of Ammonia Over Ruthenium Catalysts. *Plasma Processes Polym.* **2017**, *14*, 1600157.
(8) Xie, D.; Sun, Y.; Zhu, T.; Fan, X.; Hong, X.; Yang, W. Ammonia Synthesis and By-Product Formation From H_2O, H_2 and N_2 By Dielectric Barrier Discharge Combined With an Ru/Al_2O_3 Catalyst. *RSC Adv.* **2016**, *6*, 105338−105346.
(9) Peng, P.; Li, Y.; Cheng, Y.; Deng, S.; Chen, P.; Ruan, R. Atmospheric Pressure Ammonia Synthesis Using Non-Thermal Plasma Assisted Catalysis. *Plasma Chem. Plasma Process.* **2016**, *36*, 1201−1210.
(10) Hong, J.; Aramesh, M.; Shimoni, O.; Seo, D. H.; Yick, S.; Greig, A.; Charles, C.; Prawer, S.; Murphy, A. B. Plasma Catalytic Synthesis of Ammonia Using Functionalized-Carbon Coatings in an Atmospheric-Pressure Non-Equilibrium Discharge. *Plasma Chem. Plasma Process.* **2016**, *36*, 917−940.
(11) Aihara, K.; Akiyama, M.; Deguchi, T.; Tanaka, M.; Hagiwara, R.; Iwamoto, M. Remarkable Catalysis of a Wool-Like Copper Electrode for NH_3 Synthesis From N_2 and H_2 in Non-Thermal Atmospheric Plasma. *Chem. Commun.* **2016**, *52*, 13560−13563.
(12) Peng, P.; Cheng, Y.; Hatzenbeller, R.; Addy, M.; Zhou, N.; Schiappacasse, C.; Chen, D.; Zhang, Y.; Anderson, E.; Liu, Y.; Chen, P.; Ruan, R. Ru-Based Multifunctional Mesoporous Catalyst for Low-Pressure and Non-Thermal Plasma Synthesis of Ammonia. *Int. J. Hydrogen Energy* **2017**, *42*, 19056−19066.
(13) Akay, G.; Zhang, K. Process Intensification in Ammonia Synthesis Using Novel Coassembled Supported Microporous Catalysts Promoted By Nonthermal Plasma. *Ind. Eng. Chem. Res.* **2017**, *56*, 457−468.
(14) Akay, G. Sustainable Ammonia and Advanced Symbiotic Fertilizer Production Using Catalytic Multi-Reaction-Zone Reactors With Nonthermal Plasma and Simultaneous Reactive Separation. *ACS Sustainable Chem. Eng.* **2017**, *5*, 11588−11606.
(15) Iwamoto, M.; Akiyama, M.; Aihara, K.; Deguchi, T. Ammonia Synthesis on Wool-Like Au, Pt, Pd, Ag, Or Cu Electrode Catalysts in Nonthermal Atmospheric-Pressure Plasma of N_2 and H_2. *ACS Catal.* **2017**, *7*, 6924−6929.
(16) Mehta, P.; Barboun, P.; Herrera, F. A.; Kim, J.; Rumbach, P.; Go, D. B.; Hicks, J. C.; Schneider, W. F. Overcoming Ammonia Synthesis Scaling Relations With Plasma-Enabled Catalysis. *Nat. Catal.* **2018**, *1*, 269−275.
(17) Herrera, F. A.; Brown, G. H.; Barboun, P.; Turan, N.; Mehta, P.; Schneider, W. F.; Hicks, J. C.; Go, D. B. The Impact of Transition Metal Catalysts on Macroscopic Dielectric Barrier Discharge (DBD) Characteristics in an Ammonia Synthesis Plasma Catalysis Reactor. *J. Phys. D: Appl. Phys.* **2019**, *52*, 224002.
(18) Barboun, P.; Mehta, P.; Herrera, F. A.; Go, D. B.; Schneider, W. F.; Hicks, J. C. Distinguishing Plasma Contributions To Catalyst Performance in Plasma-Assisted Ammonia Synthesis. *ACS Sustainable Chem. Eng.* **2019**, *7*, 8621−8630.
(19) Rouwenhorst, K. H. R.; Kim, H.-H.; Lefferts, L. Vibrationally Excited Activation of N_2 in Plasma-Enhanced Catalytic Ammonia Synthesis: A Kinetic Analysis. *ACS Sustainable Chem. Eng.* **2019**, *7*, 17515−17522.
(20) Barboun, P. M.; Hicks, J. C. Unconventional Catalytic Approaches To Ammonia Synthesis. *Annu. Rev. Chem. Biomol. Eng.* **2020**, *11*, 5-1−5-19.
(21) Fridman, A. *Plasma Chemistry*; Cambridge University Press: New York, 2008; pp 92−156.
(22) Neyts, E. C.; Ostrikov, K. K.; Sunkara, M. K.; Bogaerts, A. Plasma Catalysis: Synergistic Effects At the Nanoscale. *Chem. Rev.* **2015**, *115*, 13408−13446.
(23) Snoeckx, R.; Bogaerts, A. Plasma Technology - a Novel Solution for CO_2 Conversion? *Chem. Soc. Rev.* **2017**, *46*, 5805−5863.
(24) Mehta, P.; Barboun, P.; Go, D. B.; Hicks, J. C.; Schneider, W. F. Catalysis Enabled By Plasma Activation of Strong Chemical Bonds: a Review. *ACS Energy Lett.* **2019**, *4*, 1115−1133.
(25) Rettner, C. T.; Stein, H. Effect of Vibrational Energy on the Dissociative Chemisorption of N_2 on Fe(111). *J. Chem. Phys.* **1987**, *87*, 770−771.
(26) Romm, L.; Katz, G.; Kosloff, R.; Asscher, M. Dissociative Chemisorption of N_2 on Ru(001) Enhanced By Vibrational and Kinetic Energy: Molecular Beam Experiments and Quantum Mechanical Calculations. *J. Phys. Chem. B* **1997**, *101*, 2213−2217.
(27) Murphy, M. J.; Skelly, J. F.; Hodgson, A.; Hammer, B. Inverted Vibrational Distributions From N_2 Recombination At Ru(001): Evidence for a Metastable Molecular Chemisorption Well. *J. Chem. Phys.* **1999**, *110*, 6954−6962.
(28) Diekhöner, L.; Mortensen, H.; Baurichter, A.; Jensen, E.; Petrunin, V. V.; Luntz, A. C. N_2 Dissociative Adsorption on Ru(0001): The Role of Energy Loss. *J. Chem. Phys.* **2001**, *115*, 9028−9035.
(29) Smith, R. R. Preference for Vibrational Over Translational Energy in a Gas-Surface Reaction. *Science* **2004**, *304*, 992−995.
(30) Hu, C.; Chen, X.; Jin, J.; Han, Y.; Chen, S.; Ju, H.; Cai, J.; Qiu, Y.; Gao, C.; Wang, C.; Qi, Z.; Long, R.; Song, L.; Liu, Z.; Xiong, Y. Surface Plasmon Enabling Nitrogen Fixation in Pure Water Through a Dissociative Mechanism Under Mild Conditions. *J. Am. Chem. Soc.* **2019**, *141*, 7807−7814.

https://dx.doi.org/10.1021/acscatal.0c00684
ACS Catal. 2020, 10, 6726−6734

(31) Thimsen, E. Beyond Equilibrium Thermodynamics in the Low Temperature Plasma Processor. *J. Vac. Sci. Technol., B: Nanotechnol. Microelectron.: Mater., Process., Meas., Phenom.* **2018**, *36*, No. 048501.
(32) Uytdenhouwen, Y.; Bal, K.; Michielsen, I.; Neyts, E.; Meynen, V.; Cool, P.; Bogaerts, A. How Process Parameters and Packing Materials Tune Chemical Equilibrium and Kinetics in Plasma-Based Co2 Conversion. *Chem. Eng. J.* **2019**, *372*, 1253−1264.
(33) Zhou, L. M.; Xue, B.; Kogelschatz, U.; Eliasson, B. Nonequilibrium Plasma Reforming of Greenhouse Gases To Synthesis Gas. *Energy Fuels* **1998**, *12*, 1191−1199.
(34) Eliasson, B.; jun Liu, C.; Kogelschatz, U. Direct Conversion of Methane and Carbon Dioxide To Higher Hydrocarbons Using Catalytic Dielectric-Barrier Discharges With Zeolites. *Ind. Eng. Chem. Res.* **2000**, *39*, 1221−1227.
(35) Wang, Q.; Yan, B.-H.; Jin, Y.; Cheng, Y. Investigation of Dry Reforming of Methane in a Dielectric Barrier Discharge Reactor. *Plasma Chem. Plasma Process.* **2009**, *29*, 217−228.
(36) Wang, Q.; Yan, B.-H.; Jin, Y.; Cheng, Y. Dry Reforming of Methane in a Dielectric Barrier Discharge Reactor With Ni/Al_2O_3 catalyst: Interaction of Catalyst and Plasma. *Energy Fuels* **2009**, *23*, 4196−4201.
(37) Sentek, J.; Krawczyk, K.; Młotek, M.; Kalczewska, M.; Kroker, T.; Kolb, T.; Schenk, A.; Gericke, K.-H.; Schmidt-Szałowski, K. Plasma-Catalytic Methane Conversion With Carbon Dioxide in Dielectric Barrier Discharges. *Appl. Catal., B* **2010**, *94*, 19−26.
(38) Kim, J.; Abbott, M. S.; Go, D. B.; Hicks, J. C. Enhancing C-H Bond Activation of Methane via Temperature-Controlled, Catalyst-Plasma Interactions. *ACS Energy Lett.* **2016**, *1*, 94−99.
(39) Gallon, H. J.; Tu, X.; Whitehead, J. C. Effects of Reactor Packing Materials on H_2 Production By CO_2 Reforming of CH_4 in a Dielectric Barrier Discharge. *Plasma Processes Polym.* **2012**, *9*, 90−97.
(40) Tu, X.; Gallon, H. J.; Twigg, M. V.; Gorry, P. A.; Whitehead, J. C. Dry Reforming of Methane Over a Ni/Al_2O_3 catalyst in a Coaxial Dielectric Barrier Discharge Reactor. *J. Phys. D: Appl. Phys.* **2011**, *44*, 274007.
(41) Tu, X.; Whitehead, J. Plasma-Catalytic Dry Reforming of Methane in an Atmospheric Dielectric Barrier Discharge: Understanding the Synergistic Effect At Low Temperature. *Appl. Catal., B* **2012**, *125*, 439−448.
(42) Mahammadunnisa, S.; Reddy, P. M. K.; Ramaraju, B.; Subrahmanyam, C. Catalytic Nonthermal Plasma Reactor for Dry Reforming of Methane. *Energy Fuels* **2013**, *27*, 4441−4447.
(43) Scapinello, M.; Martini, L. M.; Tosi, P. CO_2 hydrogenation By CH_4 in a Dielectric Barrier Discharge: Catalytic Effects of Nickel and Copper. *Plasma Processes Polym.* **2014**, *11*, 624−628.
(44) Zeng, Y.; Zhu, X.; Mei, D.; Ashford, B.; Tu, X. Plasma-Catalytic Dry Reforming of Methane Over γ-Al_2O_3 Supported Metal Catalysts. *Catal. Today* **2015**, *256*, 80−87.
(45) Wang, L.; Yi, Y.; Wu, C.; Guo, H.; Tu, X. One-Step Reforming of CO_2 and CH_4 Into High-Value Liquid Chemicals and Fuels At Room Temperature By Plasma-Driven Catalysis. *Angew. Chem., Int. Ed.* **2017**, *56*, 13679−13683.
(46) Michielsen, I.; Uytdenhouwen, Y.; Bogaerts, A.; Meynen, V. Altering Conversion and Product Selectivity of Dry Reforming of Methane in a Dielectric Barrier Discharge By Changing the Dielectric Packing Material. *Catalysts* **2019**, *9*, 51.
(47) Pan, K. L.; Chung, W. C.; Chang, M. B. Dry Reforming of CH_4 With CO_2 To Generate Syngas By Combined Plasma Catalysis. *IEEE Trans. Plasma Sci.* **2014**, *42*, 3809−3818.
(48) Kraus, M.; Eliasson, B.; Kogelschatz, U.; Wokaun, A. CO_2 Reforming of Methane By the Combination of Dielectric-Barrier Discharges and Catalysis. *Phys. Chem. Chem. Phys.* **2001**, *3*, 294−300.
(49) Goujard, V.; Tatibouet, J.-M.; Batiot-Dupeyrat, C. Influence of the Plasma Power Supply Nature on the Plasma-Catalyst Synergism for the Carbon Dioxide Reforming of Methane. *IEEE Trans. Plasma Sci.* **2009**, *37*, 2342−2346.
(50) Nguyen, H. H.; Kim, K.-S. Combination of Plasmas and Catalytic Reactions for CO_2 Reforming of CH_4 By Dielectric Barrier Discharge Process. *Catal. Today* **2015**, *256*, 88−95.
(51) Gibson, E. K.; Stere, C. E.; Curran-McAteer, B.; Jones, W.; Cibin, G.; Gianolio, D.; Goguet, A.; Wells, P. P.; Catlow, C. R. A.; Collier, P.; Hinde, P.; Hardacre, C. Probing the Role of a Non-Thermal Plasma (NTP) in the Hybrid NTP Catalytic Oxidation of Methane. *Angew. Chem., Int. Ed.* **2017**, *56*, 9351−9355.
(52) Hansen, F. Y.; Henriksen, N. E.; Billing, G. D.; Guldberg, A. Catalytic Synthesis of Ammonia Using Vibrationally Excited Nitrogen Molecules: Theoretical Calculation of Equilibrium and Rate Constants. *Surf. Sci.* **1992**, *264*, 225−234.
(53) Evans, M. G.; Polanyi, M. Inertia and Driving Force of Chemical Reactions. *Trans. Faraday Soc.* **1938**, *34*, 11.
(54) Bligaard, T.; Nørskov, J.; Dahl, S.; Matthiesen, J.; Christensen, C.; Sehested, J. The Brønsted-Evans-Polanyi Relation and the Volcano Curve in Heterogeneous Catalysis. *J. Catal.* **2004**, *224*, 206−217.
(55) Grabow, L. C. *RSC Catalysis Series*; RSC Catalysis Series; Royal Society of Chemistry, 2013; pp 1−58.
(56) Dahl, S.; Logadottir, A.; Jacobsen, C. J.; Nørskov, J. K. Electronic Factors in Catalysis: the Volcano Curve and the Effect of Promotion in Catalytic Ammonia Synthesis. *Appl. Catal., A* **2001**, *222*, 19−29.
(57) Snoeckx, R.; Aerts, R.; Tu, X.; Bogaerts, A. Plasma-Based Dry Reforming: A Computational Study Ranging From the Nanoseconds To Seconds Time Scale. *J. Phys. Chem. C* **2013**, *117*, 4957−4970.
(58) Akiyama, M.; Aihara, K.; Sawaguchi, T.; Matsukata, M.; Iwamoto, M. Ammonia Decomposition To Clean Hydrogen Using Non-Thermal Atmospheric-Pressure Plasma. *Int. J. Hydrogen Energy* **2018**, *43*, 14493−14497.
(59) Hansgen, D. A.; Vlachos, D. G.; Chen, J. G. Using First Principles To Predict Bimetallic Catalysts for the Ammonia Decomposition Reaction. *Nat. Chem.* **2010**, *2*, 484−489.
(60) Boisen, A.; Dahl, S.; Nørskov, J.; Christensen, C. Why the Optimal Ammonia Synthesis Catalyst Is Not the Optimal Ammonia Decomposition Catalyst. *J. Catal.* **2005**, *230*, 309−312.
(61) Aika, K.-i.; Yamaguchi, J.; Ozaki, A. Ammonia Synthesis Over Rhodium, Iridium and Platinum Promoted By Potassium. *Chem. Lett.* **1973**, *2*, 161−164.
(62) White, A. H.; Melville, W. The Decomposition of Ammonia At High Temperatures. *J. Am. Chem. Soc.* **1905**, *27*, 373−386.
(63) Hagelaar, G. J. M.; Pitchford, L. C. Solving the Boltzmann Equation To Obtain Electron Transport Coefficients and Rate Coefficients for Fluid Models. *Plasma Sources Sci. Technol.* **2005**, *14*, 722−733.
(64) Kim, J.; Go, D. B.; Hicks, J. C. Synergistic Effects of Plasma-Catalyst Interactions for CH_4 Activation. *Phys. Chem. Chem. Phys.* **2017**, *19*, 13010−13021.
(65) Mehta, P.; Barboun, P. M.; Engelmann, Y.; Go, D. B.; Bogaerts, A.; Schneider, W. F.; Hicks, J. C. *wfschneidergroup/SI-mehta-beyond-eq*; 2019; DOI: 10.5281/zenodo.3566833.

https://dx.doi.org/10.1021/acscatal.0c00684
ACS Catal. 2020, 10, 6726−6734